# Westerly Wind Events and the 1997/98 El Niño Event in the ECMWF Seasonal Forecasting System: A Case Study

FRÉDÉRIC VITART, MAGDALENA ALONSO BALMASEDA, LAURA FERRANTI, AND DAVID ANDERSON

*European Centre for Medium-Range Weather Forecasts, Reading, Berkshire, United Kingdom*

(Manuscript received 26 September 2002, in final form 20 March 2003)

ABSTRACT

The 1997/98 El Niño was one of the strongest on record. Its onset was predicted by several numerical models, though none fully captured its intensity. This was the case for the ECMWF seasonal forecasting system that underestimated the intensification during the June–July 1997 period by more than 1 K. Several strong westerly wind events developed during the onset of the 1997/98 El Niño suggesting that westerly wind events played a key role in the intensification of this El Niño. The present paper quantifies the impact of westerly wind events on the 1997/98 El Niño in the ECMWF seasonal forecasting system, through a series of experiments in which various modifications are made to convective parameterization and wind forcing to increase wind variability in the western Pacific.

The ECMWF model does not produce significant westerly wind events. A set of experiments suggests that if the model were able to simulate the May–June westerly wind event, it would have predicted significantly warmer Niño-3 (5°S–5°N, 90°–150°W) sea surface temperatures (SSTs). Increasing the convective available potential energy threshold of the cumulus parameterization significantly improves the simulation of westerly wind events and as a consequence the prediction of Niño-3 SSTs. The response of the coupled model to the wind perturbation is smaller than that in forced mode, probably due to the strong damping effect of the induced heat flux. The different ocean mean state does not seem to be responsible for the weak coupled response in the Niño-3 region.

## 1. Introduction

Predicting El Niño is of great interest since it is the most important source of potentially predictable interannual variability. The prediction of its occurrence and development represents a particularly challenging task for dynamical seasonal forecasting. Several models of intermediate complexity, based on a relatively simple representation of the equatorial Pacific Ocean and the tropical atmosphere, have been applied to this topic with some success. See, for example, Latif et al. (1998) and references therein. The performance of general circulation models to predict sea surface temperature anomalies has significantly improved in recent years and some of them provided the best real-time numerical forecasts of the 1997/98 El Niño (Trenberth 1998) although all the dynamical models considered by Barnston et al. (1999) underestimated the exceptional strength of the 1997/98 El Niño.

The European Centre for Medium-Range Weather Forecasts (ECMWF) seasonal forecasting system, based on coupled general circulation models' (GCMs') integrations, was generally rather successful in predicting the occurrence of the 1997/98 event, its maintenance and its decay a few months in advance, but forecasts initiated in April and May underestimated its intensification in June and July 1997 by more than 1 K. The main goal of the present paper is to investigate the reasons for this failure.

While the El Niño mode explains most of the interannual variability, tropical intraseasonal variability, which can be very intense in some years, is also of interest for seasonal forecasting. For example, the strong El Niño event of 1997/98 developed during a period of intense intraseasonal activity. Those variations may condition the development of warm tropical SSTs and therefore may play a substantial role in the onset and development of the El Niño–Southern Oscillation (ENSO).

Rapid changes in surface winds over the Indonesian region, known as westerly wind bursts (see, e.g., Harrison and Giese 1991) are observed on the intraseasonal timescale. The amplitude of the zonal wind anomaly is of the order of a few meters per second. It is still unclear to what extent westerly wind events are intimately related to the large-scale Madden–Julian oscillation (MJO) phenomenon. Westerly wind events tend to develop during active phases of the MJO (Zhang 1996; Lin and Johnson 1996; Chen et al. 1996), though they

*Corresponding author address:* Dr. Frédéric Vitart, European Centre for Medium-Range Weather Forecasts, Shinfield Park, Reading, Berkshire RG2 9AX, United Kingdom.
E-mail: Frederic.Vitart@ecmwf.int

can also form from paired tropical cyclones (Keen 1982) and cold surges from midlatitudes (Harrison 1984). Barnett (1984), Kessler and Kleeman (2000), and Kessler (2001) suggest that the tropical intraseasonal variability may influence the tropical climate by modulating the timing and strength of ENSO events. Fedorov (2002) and Fedorov et al. (2003) argue that El Niño behaves like an oscillatory system subject to random disturbances, which are the westerly wind events. Westerly wind events were present in the western Pacific during the onset of several recent El Niño events (Krishnamurti et al. 2000). In 1997, before the onset of the strongest El Niño recorded, several strong westerly winds events were observed (November 1996, December 1996, February–March 1997). Several papers (Slingo 1998; McPhaden 1999; van Oldenborgh 2000; Boulanger et al. 2001; Krishnamurti et al. 2000) argue that westerly wind events, possibly associated with the MJO, in late 1996 and the first half of 1997 played a crucial role in the onset and development of ENSO. Perigaud and Cassou (2000), using an intermediate coupled model, argue that the presence of westerly wind events can impact the development of an El Niño event but only if the oceanic heat content is high, as was the case in 1997 (Meinen and McPhaden 2001). Therefore, westerly wind events may be an important player in the intensification of the 1997/98 El Niño event. If this is the case, then it is important for a coupled GCM to be able to generate such wind stress variability in order to successfully forecast El Niño events months in advance.

This study explores the above hypothesis in the context of the ECMWF seasonal forecasting system. Section 2 documents the ECMWF seasonal predictions of the 1997/98 El Niño, and the ability of the ECMWF coupled system to simulate realistic MJOs and westerly wind events. In section 3, results from sensitivity experiments using fully coupled GCMs and designed to evaluate the impact of westerly wind events on El Niño in 1997 are discussed. Section 4 investigates the sensitivity to a specific change in the cumulus parameterization scheme. The relative importance of the wind and heat flux variability in the amplitude of SST anomalies is considered in section 5 by means of ocean-only experiments. Summary and conclusions are presented in section 6.

## 2. Prediction of Niño-3 SST and intraseasonal activity

The ECMWF seasonal forecasting system (Stockdale et al. 1998) is based on a coupled GCM that has been used to make an ensemble of 6-month forecasts every month from 1991 to present. At the time of the 1997/98 El Niño event the atmospheric component (IFS cycle 15R8) had a T63 spectral resolution and a 1.875° grid for surface and physical processes; there were 31 vertical levels. The ocean resolution was comparable in midlatitudes, but was increased in the Tropics to about 0.5° in the latitudinal direction so as to resolve the equatorial waves that are important for El Niño. There were 20 vertical levels of which 8 are in the upper 200 m. The atmospheric and land surface initial conditions were taken from the operational analyses/reanalyses produced by ECMWF. Ocean initial conditions were taken from an analysis of the ocean state made by forcing the ocean with the analyzed surface fluxes of momentum, freshwater, and heat while assimilating all available oceanic subsurface thermal data using the optimal interpolation scheme of Smith et al. (1991) and relaxing to surface temperature analyses (Reynolds and Smith 1994).

The atmosphere and ocean are coupled directly without flux corrections and the coupled system is integrated forward for 200 days from the initial conditions. Errors in the component models lead to a drift in the climate of the coupled system. In particular, the model produces SSTs colder than observed over most of the Pacific, Atlantic, and Indian Oceans, by up to 2°C after 6 months of integration. Therefore it is necessary to calibrate the forecasts with the climatology of the coupled GCM. To estimate the climatology of the coupled system, a set of eleven 6-month forecasts has been made from the first of each month for 6 yr of an earlier period (1991–96).

The present paper will focus on the Niño-3 (5°S–5°N, 90°–150°W) index, although the model displays slightly more skill over the Niño-3.4 region (5°S–5°N, 170°–120°W). The choice of Niño-3 was motivated by the fact that it is a widely used index for ENSO activity, and the ENSO forecasts displayed on the web from our forecasting system were based on the Niño-3 index. The ECMWF seasonal forecasting system displays skill in predicting SST anomalies over the Niño-3 region: Fig. 1 shows that the system was successful in forecasting the onset of the 1997/98 El Niño event and its decay. For forecasts started in April and May, however, the model severely underestimated the intensity of the SST warming during the months of June and July. This result is consistent with other GCM forecasts (Barnston et al. 1999; Landsea and Knaff 2000).

The period from December 1996 to June 1997 was characterized by strong tropical intraseasonal activity within which were very energetic westerly wind events (McPhaden 1999; Slingo 1998). It is likely that such strong westerly wind events perturbed significantly the equatorial ocean by creating oceanic Kelvin waves and possibly intensifying the El Niño (McPhaden 1999). The seasonal forecast system is generally deficient in representing tropical intraseasonal activity. In fact, westerly wind anomalies propagate eastwards only when they are present in the initial conditions. This is illustrated by Fig. 2 for forecasts initiated in February and March 1997. The forecasts started on 1 February do not reproduce the wind events of mid-February 1997 and especially March 1997 (Fig. 2b), whereas some aspects of the March event were captured in forecasts started on 1 March (Fig. 2c).

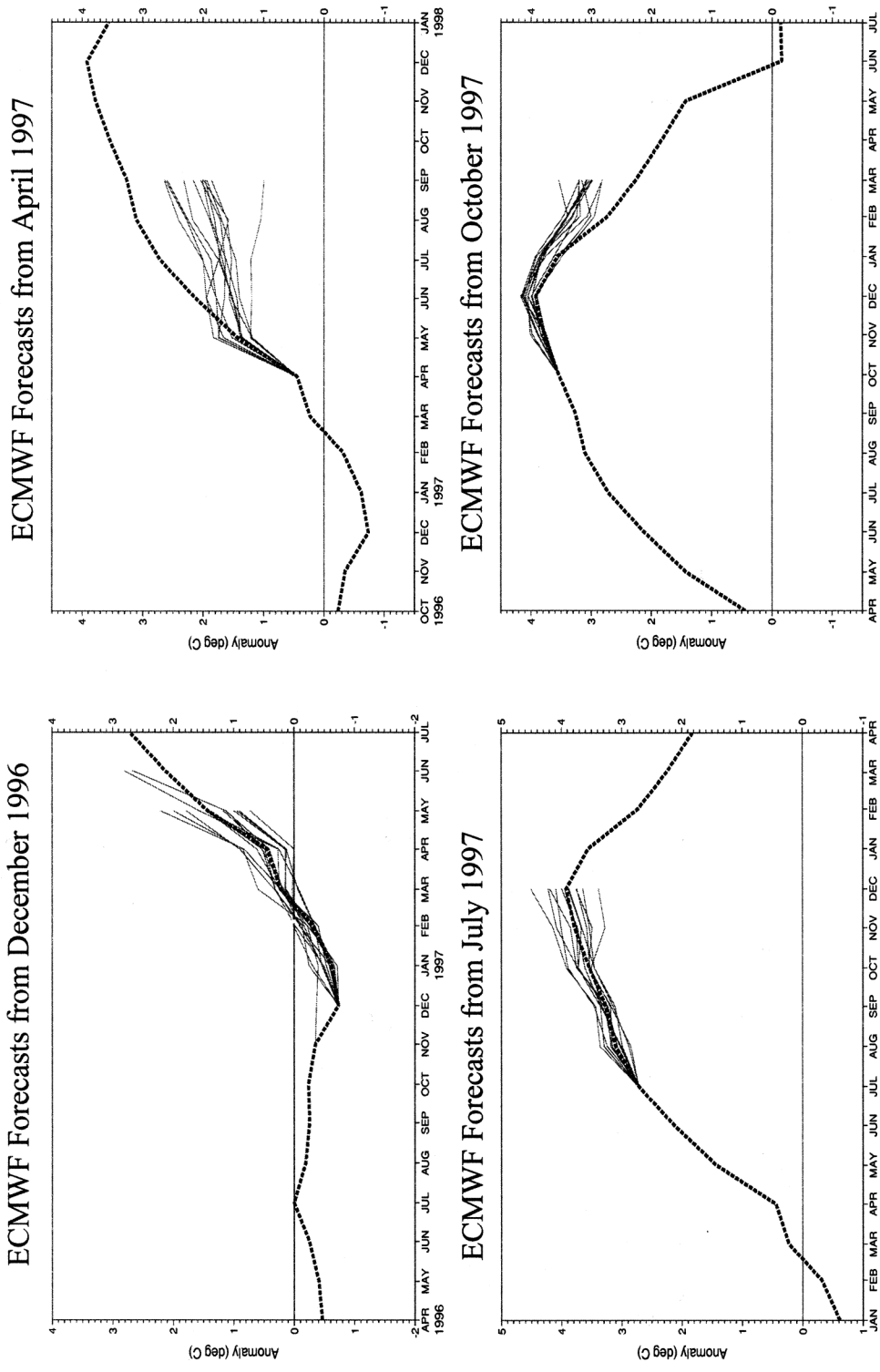


FIG. 1. Plumes of monthly mean SST anomalies predicted for the Niño-3 region (5°N–5°S, 90°–150°W). Forecasts are initialized one day apart in (top left) Dec 1996, (top right) Apr 1997, (bottom left) Jul 1997, and (bottom right) Oct 1997 and run for 184 days. Observed values are represented by the broken line. Each thin line represents one member of the ensemble.

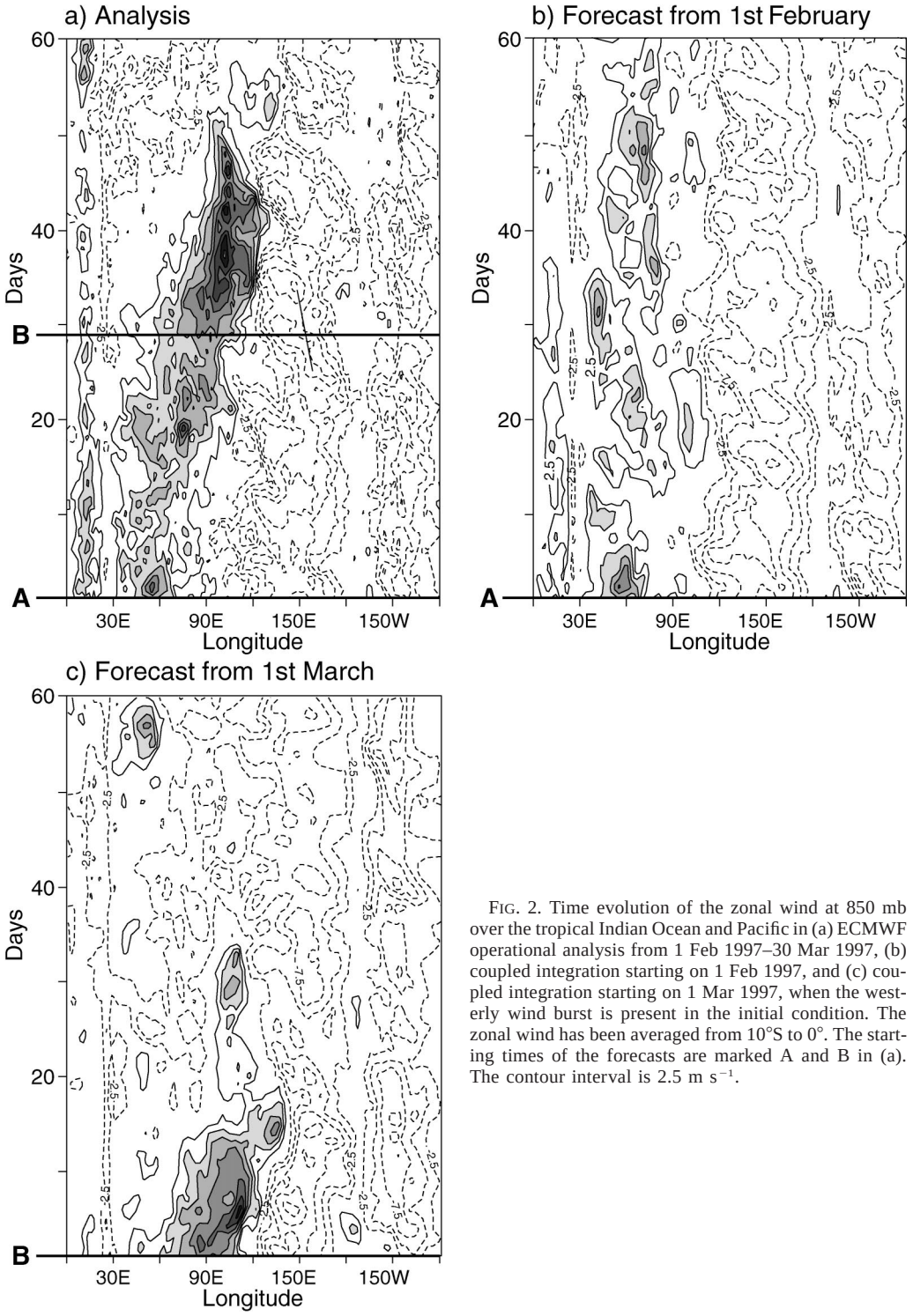


FIG. 2. Time evolution of the zonal wind at 850 mb over the tropical Indian Ocean and Pacific in (a) ECMWF operational analysis from 1 Feb 1997–30 Mar 1997, (b) coupled integration starting on 1 Feb 1997, and (c) coupled integration starting on 1 Mar 1997, when the westerly wind burst is present in the initial condition. The zonal wind has been averaged from 10°S to 0°. The starting times of the forecasts are marked A and B in (a). The contour interval is 2.5 m $s^{-1}$.

Figure 3a shows strong westerly wind events that developed from May to mid-June 1997 and propagated eastward from the Indian Ocean to as far east as 150°W, with an intensity exceeding 0.08 N $m^{-2}$. For forecasts started on 1 May 1997, not one single member of the 30-member ensemble of the ECMWF seasonal forecasting system was able to produce propagating wind events comparable to those observed. Figure 3b shows a typical ensemble member from the coupled control experiment (C_control), which will be introduced in sec-

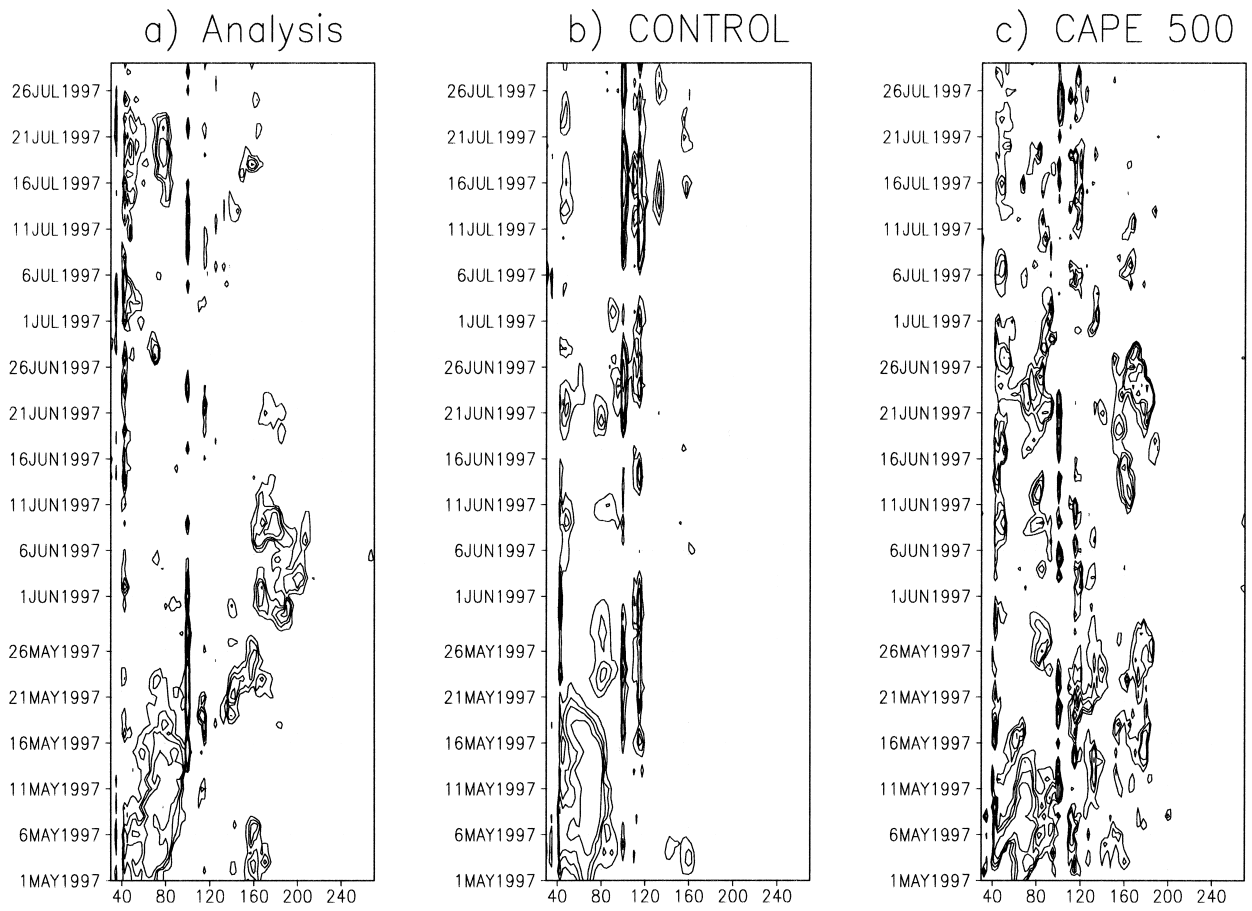


FIG. 3. Time evolution of surface zonal wind stress over the tropical Indian and Pacific Oceans (a) in ECMWF operational analysis, (b) a typical ensemble member from the C_control run, and (c) a typical ensemble member from the C_cape experiment. The wind stress has been averaged from 5°S to 5°N. Contours are 0.02, 0.04, 0.06, and 0.1 N $m^{-2}$. Values below 0.02 N $m^{-2}$ are not shown.

tion 3. It is not just the surface winds that do not show propagation. Figure 4a shows the velocity potential at 200 hPa in the ECMWF analysis, a field that is often used as a measure of MJO activity. Eastward propagation can be clearly seen. Figure 4b shows one ensemble member from C_control. No eastward propagation is evident. Analysis of other ensemble members confirms the absence of eastward propagation of MJO-like activity.

Ensembles of atmospheric-only integrations initiated with the same atmospheric initial conditions as in the coupled forecasts (from analyzed atmospheric state, soil moisture, and snow cover) and driven by observed SSTs show a similar behavior, suggesting that the lack of westerly wind events in the coupled model stems from a deficiency in the atmospheric model. Increasing the horizontal resolution of the atmospheric component of the GCM to T95, T159, and T319 does not improve significantly the simulation of the intraseasonal variability over the tropical Pacific, indicating that the problem is not simply one of resolution. Below we will, in fact, show that the problem occurs within a rather short timescale.

At ECMWF, high-resolution medium-range weather forecasts are made every day out to 10 days. These can be used to evaluate the ability of the model to simulate and predict westerly wind events up to 10 days ahead. We will concentrate on the May–June 1997 westerly wind event. Figure 5 shows plots of the surface wind for 1-, 2-, 5-, and 10-day forecasts. The dates in Fig. 5 correspond to the verifying time of the forecast. Figure 5 is not a Hovmöller diagram since it is composed of the outputs of individual forecasts with different starting dates, rather than the evolution of a single forecast. If the model could simulate equatorial winds correctly and they were predictable, then the 10-day forecasts of Fig. 5d should look like Fig. 5a, which is a good proxy of analyses. Figure 5 shows that the speed of propagation of the westerly wind event over the Indian Ocean gets slower as the forecast range increases and the amplitude is noticeably reduced (cf. e.g., Figs. 5a and 5d). The model fails to predict the transition of the westerly wind

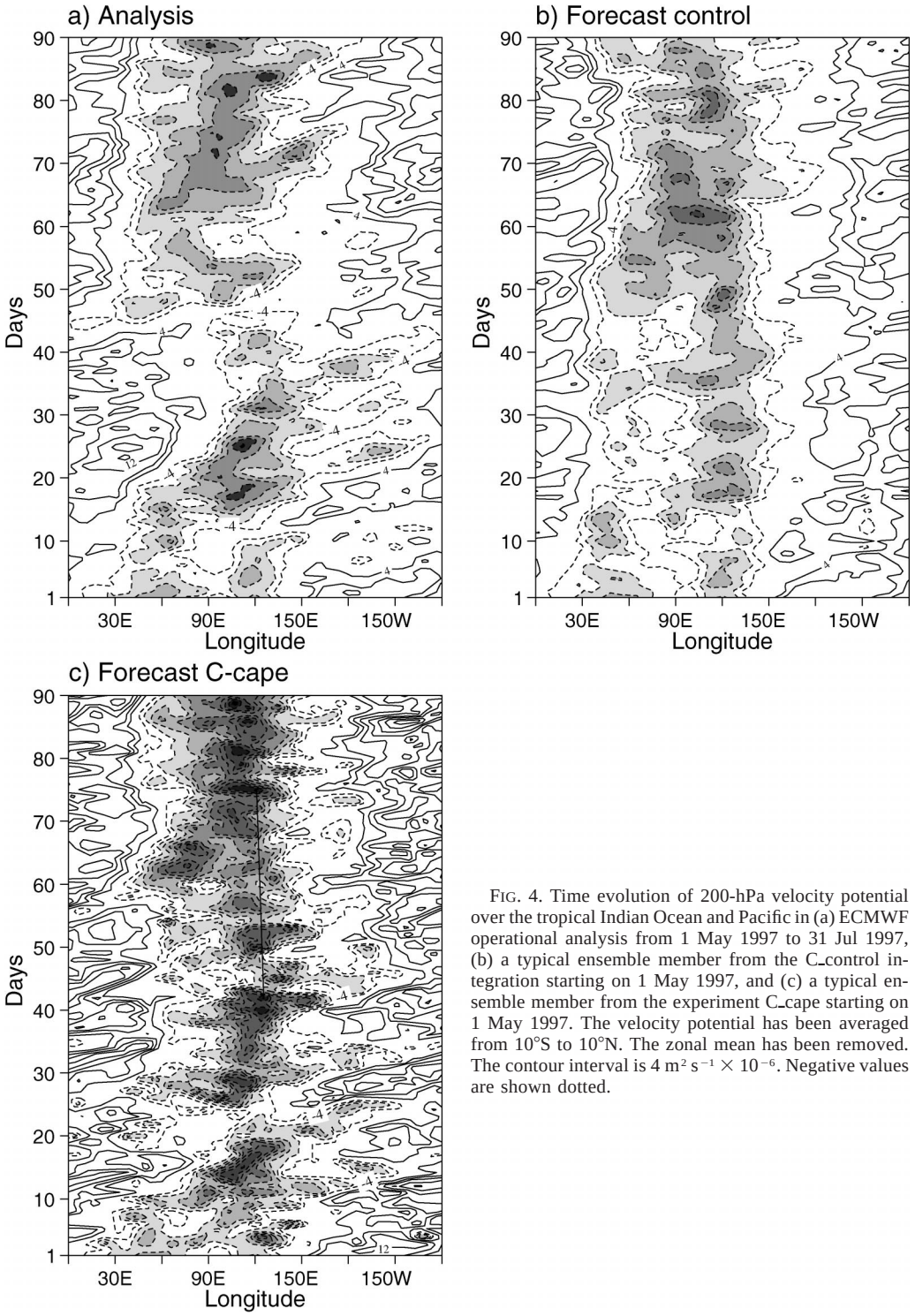


FIG. 4. Time evolution of 200-hPa velocity potential over the tropical Indian Ocean and Pacific in (a) ECMWF operational analysis from 1 May 1997 to 31 Jul 1997, (b) a typical ensemble member from the C_control integration starting on 1 May 1997, and (c) a typical ensemble member from the experiment C_cape starting on 1 May 1997. The velocity potential has been averaged from 10°S to 10°N. The zonal mean has been removed. The contour interval is 4 $m^2 s^{-1} \times 10^{-6}$. Negative values are shown dotted.

event from the Indian Ocean to the western Pacific more than 2 days in advance. In particular, it fails to predict the correct intensity over the western Pacific (between 120° and 140°E) during the period 15 May–1 June 48 h in advance (Fig. 5b) and does not predict its occurrence at all over the western Pacific 5 days in advance (Fig. 5c). However, when the initial conditions include the westerly wind event in the western Pacific, the model succeeds in predicting a westerly wind event in the central Pacific 10 days in advance (forecasts starting from 26 May to 1 June), although it does not extend as far eastward as in the analysis (Fig. 5d).

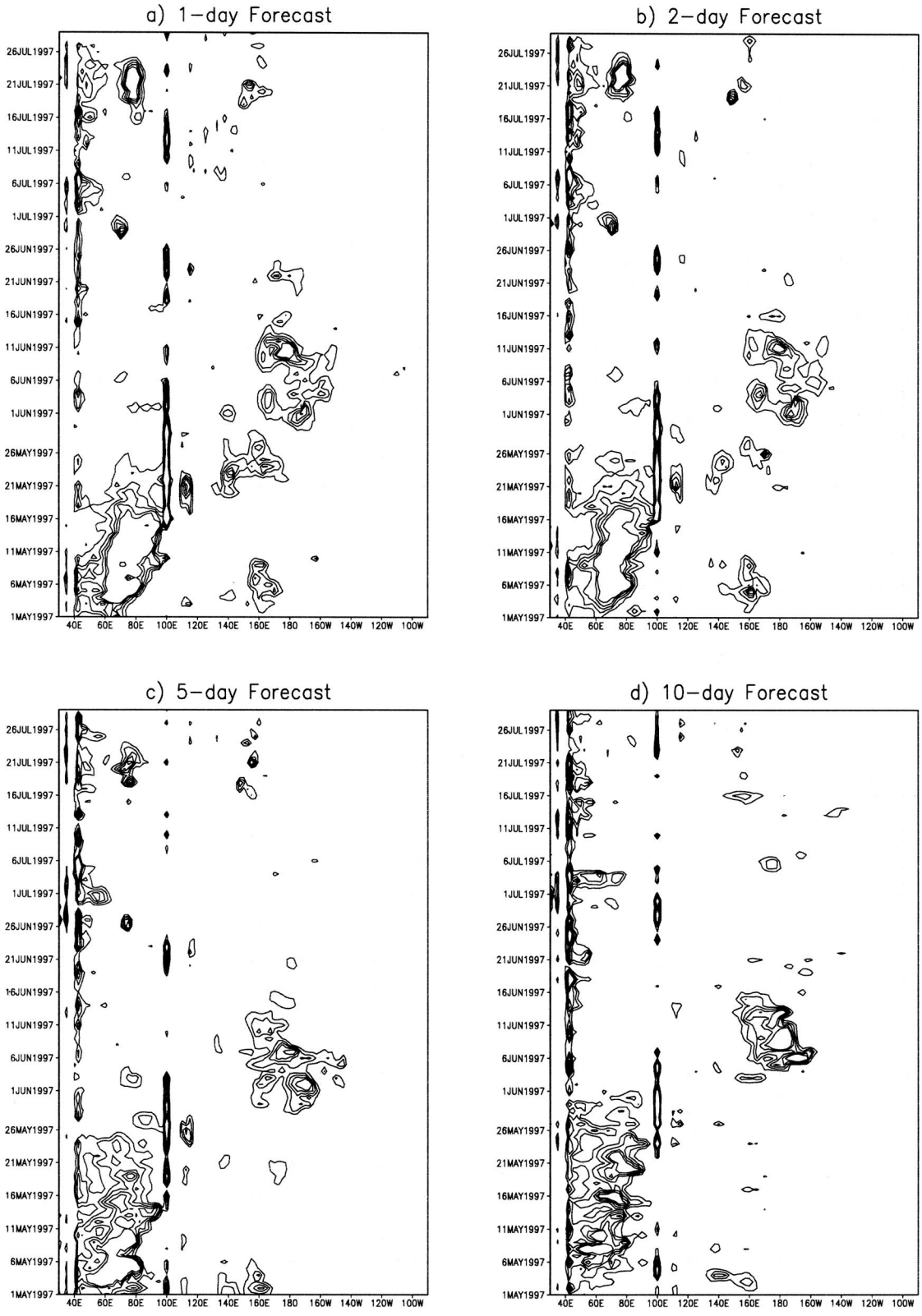


FIG. 5. Time evolution of wind stress from (a) 1-, (b) 2-, (c) 5-, and (d) 10-day forecasts from the ECMWF medium-range operational forecast system. Contour interval is 0.02 N $m^{-2}$. Only positive values are shown, starting at 0.02 N $m^{-2}$.

TABLE 1. Summary of coupled experiments.

| Expt | Calibration name | Ensemble size: Calibration | Ensemble size: Forecast | |
|---|---|---|---|---|
| C_control | C_CONTROL_CLIM | 30 | 20 | Coupled |
| C_pert | C_CONTROL_CLIM | 30 | 5 | Coupled |
| C_stoch | C_STOCH_CLIM | 30 | 20 | Coupled |
| C_cape | C_CAPE_CLIM | 30 | 20 | Coupled |
| S_control | S_CONTROL_CLIM | 30 | 20 | Semicoupled |
| S_cape | S_CAPE_CLIM | 30 | 20 | Semicoupled |

## 3. Sensitivity to the May–June 1997 wind event

In the present paper, we concentrate on the specific case of seasonal predictions initiated in May 1997. The 1 May starting date was chosen partly because the operational seasonal forecasts from May failed to predict the intensity of the El Niño and partly because it is close to the observed May–June westerly wind event. By performing additional experiments we investigate whether part of the seasonal prediction error could be related to the inadequate representation of westerly wind activity. A summary of the coupled experiments conducted is given in Table 1.

All the experiments have been performed using the same ocean component of the coupled GCM as in the operational seasonal forecasting system but with a more recent version of the atmospheric model (known as cycle 19rl). The model drift produced by this coupled ocean–atmospheric system is different from that produced by the operational seasonal forecasting system (section 2). The model SSTs in the western and central Pacific tend to be colder than observed by about 1°C and warmer than observed by about 1°C over the eastern Pacific after 3 months of integration. A 5-member ensemble of 3-month integrations has been generated in which each one is started on 1 May of each year from 1991 to 1996. These are used to create the reference climatology (C_CONTROL_CLIM) for the model forecasts, which allows the removal of model drift. A 20-member ensemble is started on 1 May 1997 to create the forecasts. The initial conditions on 1 May are obtained from the operational atmospheric and oceanic analysis systems. The ensemble is created by perturbing the initial SST by a small amount. This set of experiments is called C_control.

For forecasts started on 1 May 1997, not one single member of the 20-member ensemble of coupled integrations was able to produce propagating wind events as strong as the observed westerly wind event of May–June 1997 (one particular ensemble member is shown in Fig. 3b). There is no eastward propagation of the wind event contained in the initial conditions over the Indian Ocean in any ensemble member. The forecast Niño-3 SST anomalies, evaluated relative to C_CONTROL_CLIM, are significantly lower than observed by more than 1 K after 3 months of integration (Fig. 6), indicating that this new version of the coupled model underpredicts the ENSO development just as the operational seasonal forecasting system shown in Fig. 1.

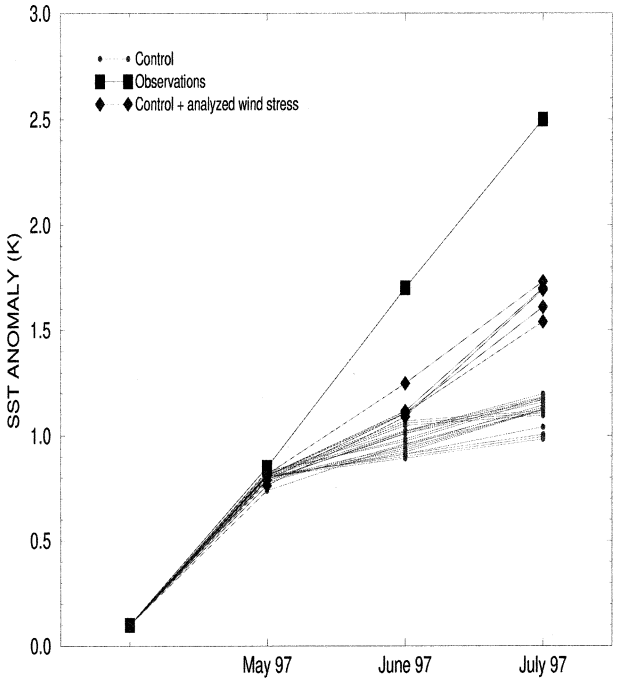


FIG. 6. Plume of monthly mean SST anomalies predicted for the Niño-3 region. Forecasts start on 1 May 1997, and the 20-member ensemble is generated by adding small perturbations on the SSTs. The squares represent the observed values, the circles represent the ensemble distribution for the control experiment (C_control), and the diamonds represent the ensemble distribution for C_pert. The values are plotted at the middle of the month.

Although much attention has been devoted to the February wind events (e.g., McPhaden 1999), the wind event in May–June was also very large. It originated in the far western Indian Ocean in April, traversed the Indian Ocean in May, weakened when it reached the Pacific, but reintensified in June. Indeed part of this westerly wind event passed far into the eastern Pacific. The impact on the ocean state was considerable. Figure 7 shows the equatorial evolution of analyzed anomalies of SST, sea level, wind stress, and heat flux for May, June, and July 1997. (The SST, wind stress, and heat flux data comes from the ECMWF atmospheric analysis system. The sea level is taken from an ocean analysis in which thermal data have been assimilated. The anomalies are computed relative to the corresponding 1991–96 analyzed climatology.) The sea level evolution shows eastward propagation of a Kelvin wave generated by the intense westerly wind anomaly in the west Pacific (around 160°–170°E) at the beginning of June. The arrival of this wave in the eastern Pacific coincides with the intensification of the SST anomaly. Could the absence of this wind anomaly in the coupled integrations account for the poor forecasts shown in Figs. 1 and 6?

An additional five-member ensemble experiment (C_pert) starting on 1 May 1997 is generated in a similar

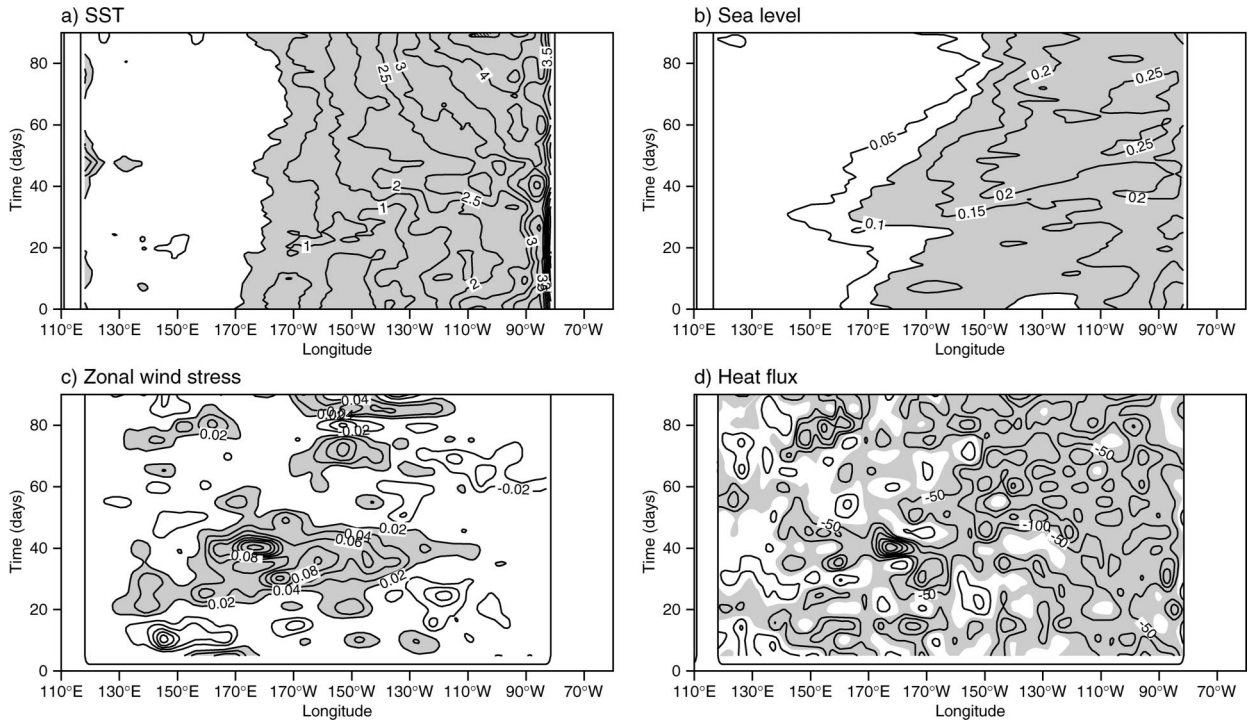


FIG. 7. Equatorial Hovmöller diagram of the analyzed anomalies in (a) SST, (b) sea level, (c) zonal wind stress, and (d) heat flux; all are with respect to the analyzed 1991–96 climatology. Contour intervals are 0.5 K, 0.5 m, 0.02 N m$^{-2}$, and 50 W m$^{-2}$, respectively. Values above 0.5 K, 0.1 m, and 0.02 N m$^{-2}$ are shaded in (a), (b), and (c), respectively; negative values shaded in (d).

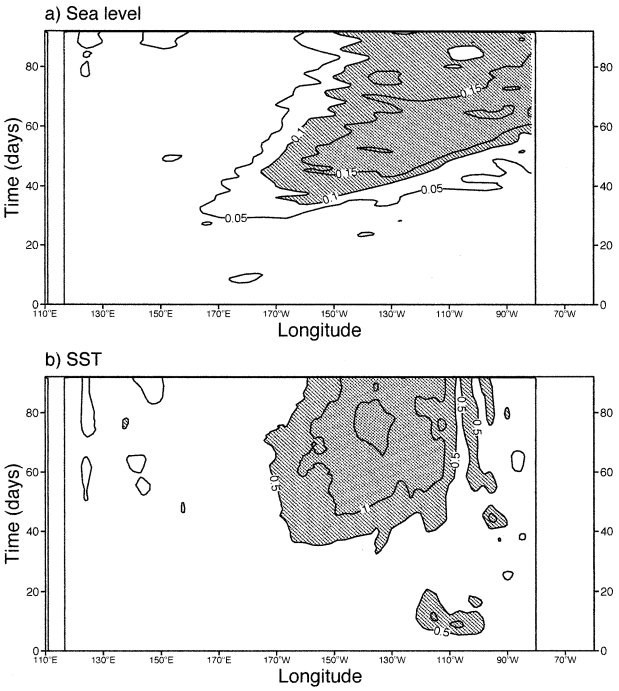


FIG. 8. (a) Time evolution of ensemble mean difference in equatorial sea surface height (m) between the perturbed and the control experiments, C_pert − C_control. Start date is 1 May 1997. Shading indicates values greater than 0.1 m. Contour interval is 0.05 m. (b) As in (a) but for potential temperature. Shading indicates values greater than 0.5 K. Contour interval is 0.5 K.

way to C_control, starting from exactly the same atmospheric and ocean initial conditions. The wind stress values from the atmospheric component of the coupled model are augmented by the observed wind stress anomalies computed from the ECMWF analysis over the tropical Pacific (20°N–20°S, 120°E–90°W) shown in Fig. 7c.

Figure 8a shows the difference in sea level between the ensemble means of the two coupled experiments C_pert and C_control. One can see a signal propagating eastward at approximately 3 m s$^{-1}$, close to the Kelvin wave speed of the first baroclinic mode. This signal is able to penetrate to the eastern boundary. The sea surface temperature plotted in Fig. 8b also shows some sign of this signal but does not show such clear propagation. Indeed, after the passage of the Kelvin wave the signal is almost a standing response. The slower behavior of the SST signal relative to sea level or depth of the 20° isotherm is well known (Barnett et al. 1993) and an explanation for that behavior has been given by McPhaden (2002). The SST signal does not extend to the eastern boundary.

Figure 8 shows that the amplitude of the SST response reaches in excess of 1.5 K in the central Pacific, though the signal averaged over the Niño-3 region is less than this value since it includes a region where the SST signal is weak. Figure 6 shows the predicted SST anomalies in Niño-3 from the coupled experiment C_pert. One can see that the latter forecasts are considerably better than

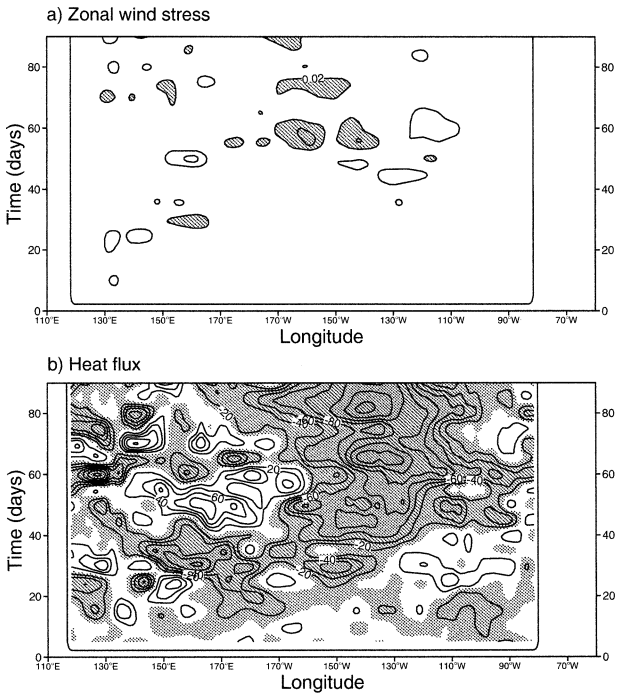


FIG. 9. Equatorial Hovmöller diagram of the coupled response to the wind perturbation ($\tau_{pert}$). (a) Coupled response in terms of zonal wind stress ($\tau$), defined as $\tau_{C\_pert} - (\tau_{C\_control} + \tau_{pert})$. (b) The heat flux (Hflx) coupled response, defined as $Hflx_{C\_pert} - Hflx_{C\_control}$. In (a) shading indicates values greater than 0.02 N m$^{-2}$, and the contour interval is 0.02 N m$^{-2}$. In (b) negative values are shaded and the contour interval is 20 W m$^{-2}$.

those in C_control but are still weaker than the observed amplitude.

The changes in SST induced by the imposed winds in turn generate new winds and heat fluxes. Figures 9a and 9b show the changes in wind and heat flux induced by the SSTs resulting from the wind perturbation and illustrate the character of the coupled interactions in the model. Over the central and eastern Pacific, the stresses are broadly in line with expectation in that there is anomalous convergence over the area of warm SST anomalies. The effect of these winds on SST will be discussed in section 5b.

One might have guessed that the development of such a large El Niño as in 1997 would have had some help from the heat fluxes during the development phase (i.e., a positive heat flux anomaly) but it appears that this was not so in the coupled model. The observed SST and heat flux anomalies from the ECMWF analysis system are shown in Figs. 7a and 7d, respectively. They confirm that the heat flux was negative throughout this period. The ratio between heat flux anomalies and SST anomalies for the C_pert experiment is about $-80$ W m$^{-2}$ K$^{-1}$ over the eastern Pacific, with a close link between the regions of maximum anomalous SST and maximum heat flux (cf. Figs. 8b and 9b). The spatial structure of the analyzed heat flux in Fig. 7d does not mirror the SST anomaly of Fig. 7a to the same extent as in the C_pert experiment, and the link between anomalous SST and anomalous heat flux in the analysis seems weaker than in the coupled model, at about $-40$ W m$^{-2}$ K$^{-1}$. In addition, observational studies indicate a damping rate on an intraseasonal timescale of about 20 W m$^{-2}$ K$^{-1}$ (McPhaden 2002). This suggests that the negative feedback from the heat flux in the coupled model may be too strong. The role of heat fluxes will be discussed further in section 5.

The previous experiments suggest that it is necessary for the atmospheric model to simulate westerly wind events in order to be successful in simulating the intensification of the 1997/98 El Niño event. Several methods of increasing the model variability are possible. One consists of adding stochastic perturbations to each member of the ensemble throughout the duration of the forecast. An example of such a technique is the use of stochastic physics (Palmer 2001), where gridpoint tendencies in the physics of the atmospheric model are randomly perturbed. For each ensemble member, the stochastic physics perturbs gridpoint tendencies of the physics up to 50%. The tendencies are multiplied by a random factor drawn from a uniform distribution between 0.5 and 1.5. The random factor is constant within a 10° × 10° domain, for 6 h. The whole globe is perturbed.

A 20-member ensemble of forecasts with stochastic physics was performed starting on 1 May 1997. This will be denoted C_stoch. Since stochastic physics might perturb the model reference climatology, a new set of hindcasts spanning the period 1991–96 was necessary. This climatology is denoted C_STOCH_CLIM. The 97 anomalies measured relative to this climatology are shown in Fig. 10a. Comparison with Fig. 6 indicates a spread of C_stoch ensemble much larger than in the C_control. Several members of the ensemble display a warming stronger than any member of the C_control run, and not too far from the warming obtained when adding observed wind perturbations. No member approaches the observed warming, however.

While stochastic physics creates perturbations of the surface wind, it is unlikely that these will resemble westerly wind events. Stochastic physics perturbations would be applied independently of the fact that we know there will be a westerly wind event, and therefore a part of the predictability is lost. Modifying the physics of the atmospheric model in such a way that it can create and maintain westerly wind events should be a better approach since any predictability of westerly wind events would then be taken into account. The next section explores this approach.

## 4. Sensitivity to the cumulus parameterization

The deep convection scheme used in the present model is a mass-flux scheme described in Tiedtke (1989). The scheme is designed to minimize the convective available potential energy (CAPE), the closure being

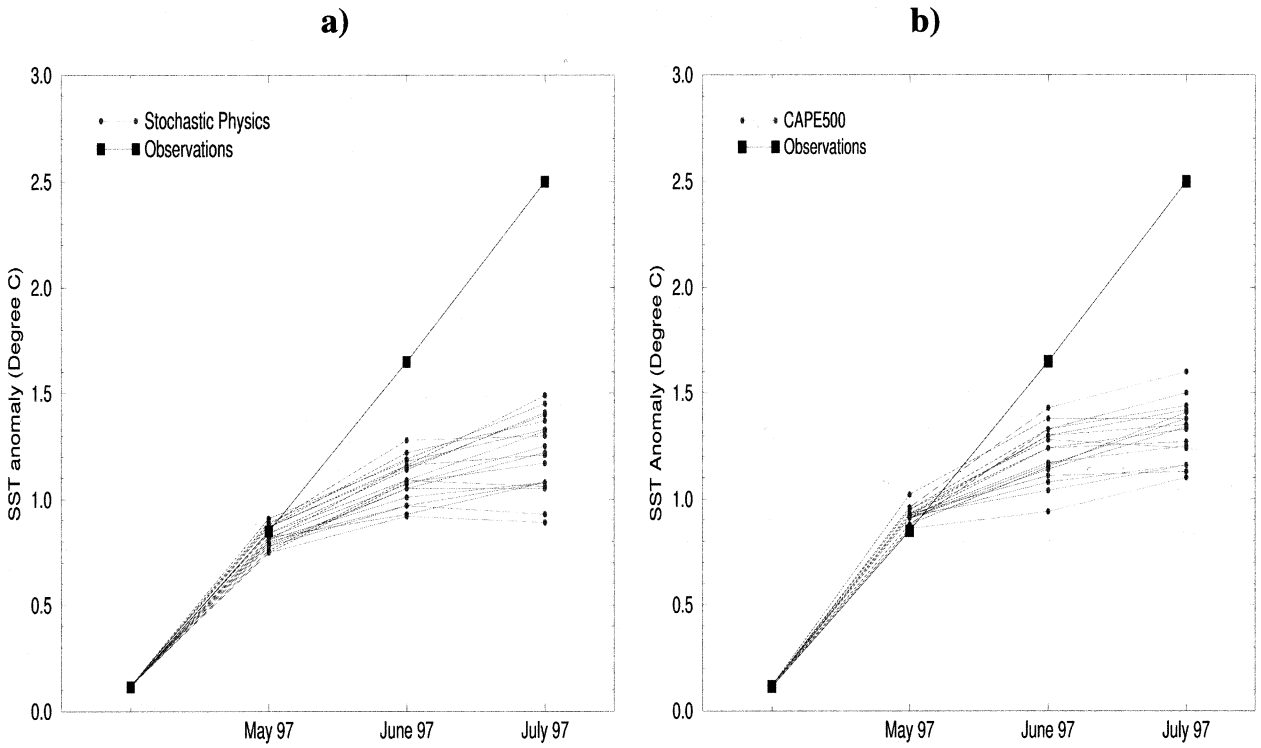


FIG. 10. Plume of monthly mean SST anomalies predicted for the Niño-3 region. Forecasts are initialized on 1 May 1997, and the 20-member ensemble is generated (a) by adding stochastic perturbations to the physics parameterization and (b) by using C_cape. The squares represent the observed values.

the condition that the CAPE should be zero. There is no observational evidence that such a condition should apply in the real world. Increasing the threshold of the CAPE is known to significantly impact the transients in the model (Vitart et al. 2001). Lin and Neelin (2000) have proposed using different values of the CAPE threshold to generate an ensemble of perturbations. Tests with different values of CAPE threshold indicate that the change in the convective parameterization becomes significant when the CAPE threshold exceeds a value of the order of 200 J $kg^{-1}$. As the main focus of the following experiments is to find out if the variability of the ECMWF model is sensitive to the CAPE threshold, a value of 500 J $kg^{-1}$ was chosen, though this may be higher than can be rigorously justified. The choice of 500 J $kg^{-1}$ for the CAPE threshold will be referred as CAPE500 hereafter.

Part of the failure of the present system to develop intraseasonal variability may be due to the fact that the simulated atmosphere is too stable. Having a CAPE threshold greater than zero delays the onset of deep convective adjustment parameterization allowing the model to become more unstable and to perform more of this role explicitly.

As for the previous experiments, a 20-member ensemble of 3-month integrations starting on 1 May 1997 has been generated with the CAPE500 choice (C_cape runs). In addition, a calibration set consisting of five-member ensembles of coupled integrations using the same CAPE500 threshold and starting on 1 May 1991–1996 has been created to sample the related climatology C_CAPE_CLIM. Changes in the physics of the model have a significant impact on the mean state and on the drift of the coupled model. For example, the SSTs produced by C_CAPE_CLIM with 1 May as forecast starting date are colder than that of C_CONTROL_CLIM in the Niño-3 region during the 3 months of integrations (Fig. 11). The atmospheric mean state simulated by the C_CAPE_CLIM is not significantly better than the one from the C_CONTROL_CLIM. The impact of delaying the convective activity depends on the season. Additional experimentation based on uncoupled simulations has shown that winter CAPE500 simulations have an improved mean atmospheric circulation but those started in spring–summer showed a degraded mean circulation.

The C_cape experiments display a significantly increased variability of the wind stress over the tropical Pacific. Whereas the C_control runs were unable to create strong eastward propagation of wind events in the central western Pacific, C_cape runs can create westerly wind events near the date line with an amplitude comparable to observations. Figure 3c shows one such example. The eastward propagation can also be seen in terms of velocity potential at 200 hPa from a coupled C_cape integration starting on 1 May 1997 (Fig. 4c). The eastward displacement of deep convection in the

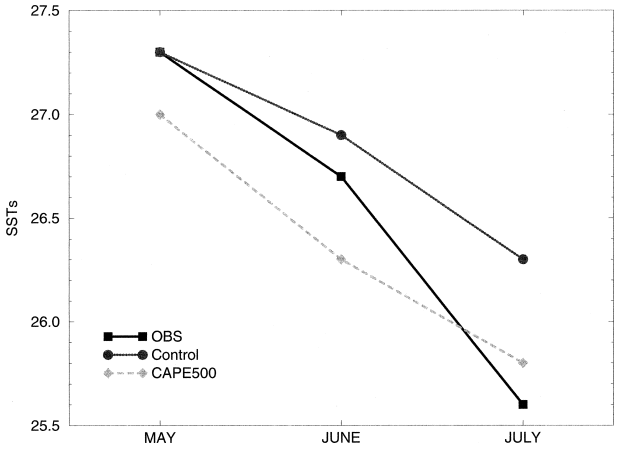


FIG. 11. Mean SSTs averaged over the Niño-3 region and over the period 1991–96. The squares represent the observed mean SSTs, the circles represent the mean of the control integrations starting on 1 May, and the diamonds represent the mean of the CAPE500 integrations starting on 1 May. The CAPE500 integrations generate colder SSTs in the Niño-3 region than the control experiment. CAPE500 displays a cold bias during the first 2 months of integrations in Niño-3, whereas the control experiment generates a warm bias.

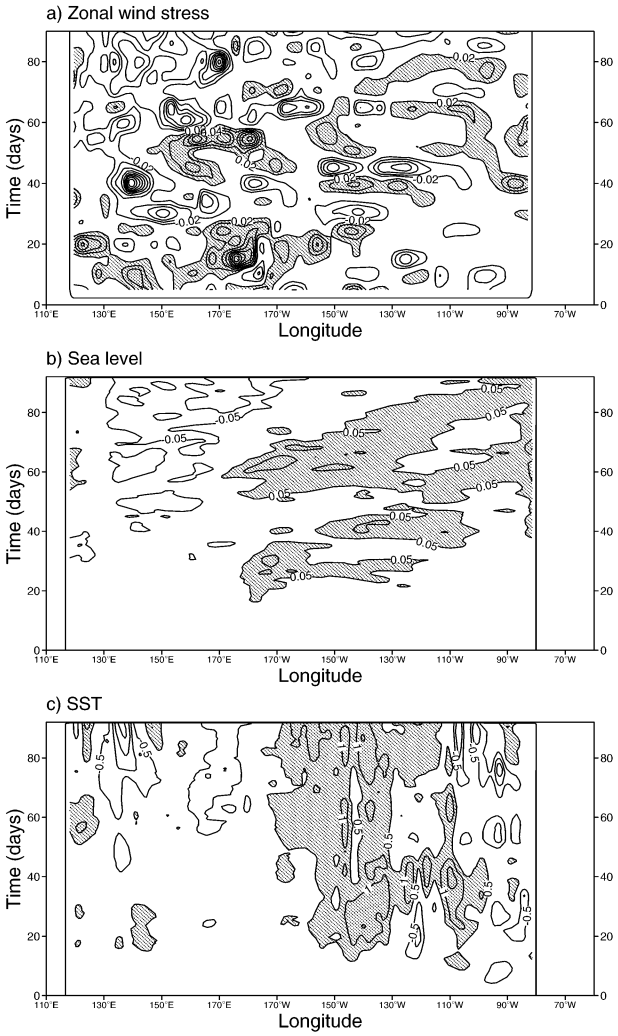


FIG. 12. Time evolution of the best C_cape minus best C_control anomalies of (a) surface stress, (b) sea level, and (c) potential temperature in the member of the CAPE500 ensemble that gives the strongest warming over the Niño-3 region. In (a) the contour interval is 0.02 N $m^{-2}$ and values greater than 0.02 N $m^{-2}$ are shaded; in (b) the contour interval is 0.05 m, with values greater than 0.05 m shaded; and in (c) the contour interval is 0.5 K with values larger than 0.5 K shaded.

tropical Pacific is reminiscent of the Madden–Julian oscillation, though the speed of propagation is too large. This seems to be a clear improvement in comparison to experiment C_control (Fig. 4b), though still not fully realistic. However, not a single member of the 20-member ensemble of C_cape started on 1 May 1997 creates a westerly wind event extending as far eastward as observed in June 1997. Nevertheless, the C_cape experiments can be used as sensitivity experiments to evaluate the impact of westerly events on the SST variability. The 20-member C_cape ensemble initiated on 1 May 1997 shown in Fig. 10b displays a warming of SST larger than the control ensembles (Fig. 6) (95% significant according to the Wilcoxson–Mann–Whitney test, e.g., Wonnacott and Wonnacott 1977). The ensemble mean is still far from the observed warming, but some members of the ensemble create a warming close to that obtained when the observed westerly wind anomalies are imposed on the ocean.

All 20 members of the ensemble predict westerly wind events in the first two months of integrations, though the intensity and timing varies considerably from one member to the next. The ensemble members that create the strongest warming over Niño-3 coincide with the members exhibiting the strongest westerly wind events. Three-month averages of Niño-3 SSTs and zonal winds averaged over the central Pacific region (5°N–5°S, 160°E–180°) are significantly correlated (correlation of 0.7), suggesting that the westerly wind events in the model have a significant impact on the Niño-3 SSTs. Figure 12 shows a Hovmöller diagram of the time evolution of the difference in SSTs, sea level, and wind stress between the best C_cape and the best C_control (best meaning the ensemble members that produced the strongest warming in the Niño-3 region). The difference in Niño-3 SSTs between the two sets of experiments can be traced back to the occurrence of two westerly wind events, in May and June, that propagated eastward well beyond the date line. The impact of those westerly wind events on the ocean state can be seen in the sea level (Fig. 12b) as eastward propagating Kelvin waves and in the SST warming that appears to the east of the wind anomaly (Fig. 12c). This suggests that the ability of C_cape simulations to create westerly wind events is the main reason for the improvement in the Niño-3 forecasts. Some improvements with C_cape may be due to a different mean state as shown in Fig. 11. In section 5, we will consider the impact of the drift, and in section

5b we will evaluate the impact of the wind variability produced in C_cape when acting on a different oceanic mean state, with experiments involving ocean-only runs.

To evaluate the influence of the SST drift in Fig. 11 on the Niño-3 forecasts shown in Fig. 10, experiments have been generated in which the atmosphere sees the observed SSTs, whereas the ocean is forced by the fluxes produced by the atmosphere. Two sets of experiments, S_cape and S_control, have been generated with and without the change in the CAPE threshold. The results obtained in this framework are consistent with those obtained when the atmosphere and ocean are fully coupled; that is, in experiments S_cape the SST warming produced by the ocean model in the Niño-3 region is significantly larger than in the corresponding S_control experiments. Since the atmosphere is driven by observed SSTs in these experiments, the drift in SSTs in the ocean model has no impact on the simulated atmospheric intraseasonal variability. Therefore, the difference in the SST anomalies predicted by the ocean model between S_cape and S_control runs does not result from the difference in SST drift.

In addition to the coupled integrations referred to above, additional experiments using the atmospheric model only and forced by prescribed SSTs have been performed. Some of these were carried out for ''perpetual March'' conditions, both for the standard and CAPE500 cumulus parameterizations, and are denoted A_control and A_cape, respectively. A major impact of CAPE500 parameterization is the significant increase of energy in the 40–50-day band apparent in the A_cape integrations. A power spectrum of equatorial velocity potential from A_cape runs shows a relative maximum for variations with periods around 40 days, not too far from the observed period of the Madden–Julian oscillation (Fig. 13). Results from the A_control integration are also shown for comparison. A less desirable feature in the A_cape integrations is the increase in energy at periods shorter than 10 days.

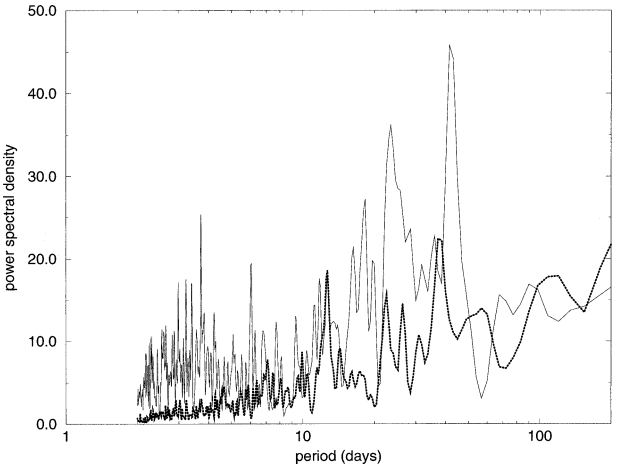


FIG. 13. Zonal wavenumber-1 equatorial velocity potential computed from 3-yr integrations of the atmospheric model using perpetual Mar SSTs. The control run is the heavy dotted line and CAPE500 is the thin full line.

*Conclusions from CAPE experiments*

The previous sections have discussed the impact of westerly wind events on the SST in the Niño-3 region in 1997. Modifying the convective cumulus parameterization in such a way that it produces a more realistic spectrum of westerly wind events, improves significantly the forecast for the year 1997. However, the overall skill over the period 1991–96 appears similar for C_control and C_cape experiments starting on 1 May, with comparable linear correlation and rms error when compared with observations.

All 20 members of the C_cape forecast ensemble produce westerly wind events when started on 1 May 1997, although their intensity and timing vary considerably from one member of the ensemble to another. Interestingly, only 25% of C_cape runs starting on 1 May of each year from 1991 to 1996 and covering the period 1 May–31 July display westerly wind events. This behavior is not unreasonable since no significant westerly wind events were observed between May and July over these years in the central Pacific. In particular, no ensemble member starting on 1 May 1995 and 1996 produced a westerly wind event in the central Pacific. This suggests that the westerly wind events in May–June 1997 may have some predictability, and may explain why the C_cape experiment produces better forecasts for 1997 than stochastic physics.

Ensembles with stochastic physics present a larger spread than the C_cape ensemble, since it includes the possibility that there are westerly wind events or there are no westerly wind events. The best forecast with stochastic physics is comparable to the best forecast with CAPE500, but the worst forecast with stochastic physics, which does not include any westerly wind event, is clearly worse than the worst forecast with CAPE500. An ensemble of integrations with both stochastic physics and a 500 J $kg^{-1}$ CAPE threshold produces results comparable to the results of the experiment with stochastic physics alone, and therefore worse than with CAPE500 alone. Therefore, stochastic physics seems to have a positive impact on the Niño-3 SST forecasts when the atmospheric model does not display any significant intraseasonal variability in the wind stress, but may lower the skill of the forecasts when the model displays some skill in simulating westerly wind events.

## 5. Ocean-only experiments

### *a. The ocean response to the observed anomalous conditions*

In order to quantify the effect on the SST of the different anomalous conditions observed during May–July 1997, a series of ocean-only experiments was con-

TABLE 2. Summary of experiments conducted to measure the impact of the different anomalous conditions on SST evolution during May, Jun, Jul 1997. ''Clim'' stands for the 1991–96 climatology for the given variable.

| Expt | Wind | Heat | $P - E$ | Ocean initial conditions | Comparison |
|---|---|---|---|---|---|
| O_anal | Analysis | Analysis | Analysis | Analysis | FOR_CLIM |
| O_notaux | Clim | Analysis | Analysis | Analysis | O_anal |
| O_nohflx | Analysis | Clim | Analysis | Analysis | O_anal |
| O_nopme | Analysis | Analysis | Clim | Analysis | O_anal |
| O_nooic | Analysis | Analysis | Analysis | Clim | O_anal |

ducted in which the ocean model was forced using different surface fluxes and ocean initial states. Each integration started on 1 May 1997 and lasted for 3 months. To create a reference climatology (FOR_CLIM), the ocean model was forced by analyzed fluxes for 3 months starting from 1 May of each year during the period 1991–96. The ocean initial conditions were the same as those used in the coupled experiments. This way of creating a forecast and a reference climatology mimics the method used in the coupled experiments. The forcing fields consisted of wind stress, heat, and freshwater fluxes derived from ECMWF reanalysis until December 1993 and from NWP operational analysis thereafter (denoted ERA/ops). A summary of the experiments conducted is given in Table 2.

In experiment O_anal, which acts as a control experiment, the forcings are the analyzed fluxes for May, June, and July 1997 and the ocean initial conditions are those for 1 May 1997. This represents the best possible attempt to reproduce the observed SSTs. The anomalous wind and heat flux are shown in Figs. 7c and 7d, respectively. If the forcing, the ocean model, the initial conditions, and the climatology (FOR_CLIM) were all perfect, the resulting SST anomaly in the forced ocean integration would be equal to that observed. By comparing the SST anomaly from experiment O_anal with the analyzed SST anomaly (Fig. 14a with Fig. 7a), one can see that this is not the case: the ocean model produces an SST signal that peaks at a longitude around 125°W compared to 100°W in the observations, and its maximum is about 1 K weaker than observed. In the west Pacific a cold anomaly of 0.5–1 K is present in Fig. 14a that is not present in the observations. On the other hand, we find that the intensity of the sea level and thermocline anomalies in experiment O_anal are in good agreement with the anomalies in the ocean analyses in which all thermal data have been assimilated: the magnitude of the errors is about 2 cm in sea level and 10 m in thermocline depth, that is, less than 10% the value of the interannual anomaly. If we take the ocean analysis as a measure of truth, then, since the model reproduces well the analyzed sea level and thermocline depth anomalies, we conclude that the dynamical response of the model to the interannual variability of the wind is largely correct. A visual inspection of the anomalous subsurface temperature indicates that the difference between experiment O_anal and the observed state is confined to the upper 50 m, suggesting that the deficiencies in the simulation of the SST anomalies may be attributed to surface processes such as heat fluxes and/or mixing within the mixed layer.

The SST anomaly produced by the model is the response to four different anomalous conditions: wind stress, heat flux, freshwater, and initial conditions. To quantify the contribution of each of these to the evolution of SST, we have carried out four different experiments O_notaux, O_nohflx, O_nopme, and O_nooic, in which the effect of withdrawing the component in question is assessed by replacing the anomalous conditions over the tropical Pacific within 20° of the equator by their corresponding climatological values.

The contribution of the anomalous wind can be measured by comparing experiment O_anal with experiment O_notaux. Figure 14b shows the SST differences between these two experiments. The effect of the wind is only apparent after 40 days into the integration. The peak value of the SST difference is greater than 3.5 K in the central eastern Pacific. In the western Pacific the wind does not seem to be responsible for the cooling noted in Fig. 14a. The effect of the wind anomaly on the sea level (not shown) is consistent with the observed behavior, as documented by Kutsuwada and McPhaden 2002, and it is similar to the effect of the wind perturbation in the coupled experiments shown in Fig. 8a.

In experiment O_nohflx, the heat flux anomaly over the tropical Pacific has been removed, and therefore only climatological heat flux is used over this area; in all other respects it is like experiment O_anal. The contribution of the anomalous heat flux to the SST, as measured by the difference between experiment O_anal and O_nohflx, is shown in Fig. 14c. The heat fluxes have a damping effect, which is particularly strong in the eastern Pacific, over the area of maximum observed SST anomaly shown in Fig. 7a. The cooling induced in the far east reaches 2.5 K. In the eastern Pacific the pattern of influence of the heat flux on SST is similar to the error in SST in experiment O_anal (Fig. 14a − Fig. 7a), suggesting that the anomalous heat flux from the atmospheric analysis might be in error. The effect of the heat flux anomaly, however, is not restricted to the eastern Pacific, but extends westward as far as 140°E, producing a cooling of 1 K around 155°E during the third month. The effect of the heat flux anomaly effect on sea level and depth of the 20°C isotherm (D20) is small.

The effect of the anomalous ocean initial conditions can be measured by the difference between experiment

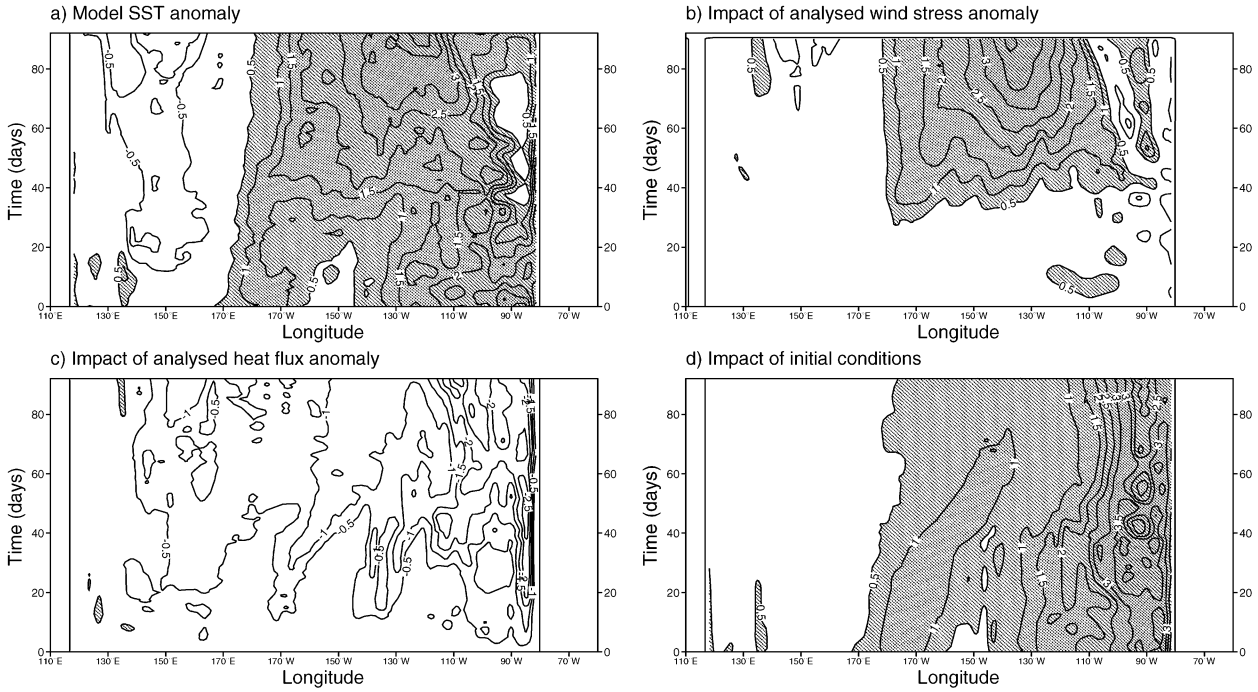


FIG. 14. Time evolution of the equatorial SST differences between experiments. (a) O_anal and FOR_CLIM, (b) O_anal and O_notaux, (c) O_anal and O_nohflx, (d) O_anal and O_nooic. The contour interval is 0.5 K; values greater than 0.5 K are shaded.

O_anal and 0_nooic. The latter uses the climatological mean state for the ocean obtained by averaging the ocean initial states for 1 May for each year from 1991 to 1996. Figure 14d shows that the anomalous ocean initial conditions contributes to the SST warming all along the equator with a maximum contribution of 3–3.5 K east of 110°W, and remains throughout the integration.

Vialard et al. 2002 suggest that $P - E$ forcing played a significant role in the SST variability during the 1997/98 El Niño event, especially in the vicinity of the eastern edge of the warm pool. In our experiments, however, the effect of the anomalous $P - E$ forcing is small in all the fields, namely less than 0.2 K in SST, less than 2 cm in the sea level, and less than 5 m in D20, and so is not shown.

### *b. The ocean response to forcing from coupled experiments*

In sections 2 and 3 we described how the coupled model underpredicted the full intensity of the SST anomaly and assessed the model sensitivity to wind perturbations. The results suggested that the failure of the coupled model to forecast the correct SST amplitude was largely due to the lack of wind variability. However, Fig. 6 showed that, even when the full wind stress anomaly was included, the SST anomaly was still underpredicted by the coupled model. Further, in the previous section we showed that the SST response to the anomalous wind stress in the ocean-only experiments (3.5 K in Fig. 14b) was more than double the response obtained in the coupled experiment C_pert (1.5 K in Fig. 8b). These facts point to other deficiencies in the coupled model. For example, a different ocean mean state in the coupled system can influence the wave propagation as suggested by Benestad et al. (2002). Additional coupled interactions can result from changes in the SST. Therefore, an additional set of experiments was conducted in ocean-only mode in which the anomalous atmospheric forcing from the coupled model experiments was superimposed on the climatological forcing FOR_CLIM. A first set of experiments was designed to measure the nonlinear effects of the ocean mean state of the coupled model on the development of SST anomaly. A second set was designed to quantify the strength of the ''coupled interactions.'' A summary of these experiments is given in Table 3.

To measure the nonlinear impact of the ocean mean state of experiment C_control on the SST evolution, experiment Ocx_ch was carried out in which both the anomalous wind stress and heat fluxes from five ensemble members of the coupled integrations C_control are superimposed on the analyzed flux climatology (FOR_CLIM). Experiments C_control and Ocx_ch have therefore the same anomalous forcing (in terms of wind and momentum) superimposed on different mean flux climatologies (C_CONTROL_CLIM and FOR_CLIM, respectively). Assuming that the effect of $P - E$ on SST is small, the differences between anomalies in Ocx_ch and C_control will be indicative of the effect of the

TABLE 3. Summary of set of ocean experiments conducted to isolate the impact of the different components of coupled fluxes. Each consists of an ensemble of five ocean integrations.

| Expt | Anomaly | | Mean state |
|---|---|---|---|
| | Wind | Heat | |
| C_control | C_control | C_control | C_CONTROL_CLIM |
| Ocx_ch | C_control | C_control | FOR_CLIM |
| Ocx | C_control | Analysis | FOR_CLIM |
| Oc500x | C_cape | Analysis | FOR_CLIM |
| Oix | Fig. 9a | Analysis | FOR_CLIM |
| Oih | Analysis | Fig. 9b | FOR_CLIM |

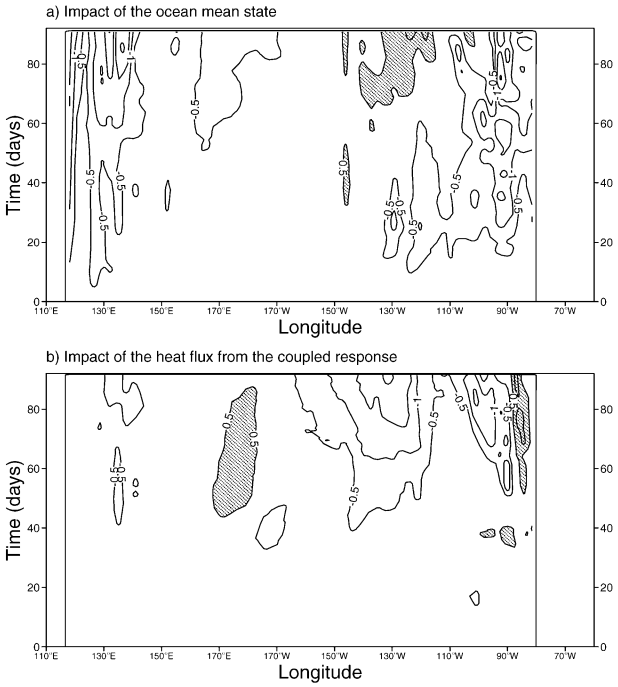


FIG. 15. Impact on the evolution of the equatorial SST anomaly of (a) the mean state, as measured by the differences between the anomalies from experiments Ocx_ch and C_control (each anomaly referred to its respective climatology), and (b) the heat flux from the ''coupled response'' (depicted in Fig. 9b), as measured by the difference between experiments Oih and O_nohflx. Contour interval is 0.5 K; values over 0.5 K are shaded.

ocean mean state (the anomalies are calculated with respect to their respective oceanic mean states FOR_CLIM and C_CONTROL_CLIM). In the absence of nonlinear interactions, the anomalies from Ocx_ch and C_control would be identical. Results indicate that the differences between the equatorial SST anomalies from these experiments hardly exceed 0.5 K in the central Pacific (Fig. 15a). The mean state has largest impact in the western Pacific (west of 150°E) and in the far eastern Pacific (east of 110°W), where the coupled mean state favors the development of larger warm anomalies than the forced mean state. Therefore, it can be concluded that the weak SST response to the wind perturbation in experiment C_pert cannot be attributed to the coupled drift. Similar experiments conducted using the forcing from the C_cape experiment confirm that the improvement of the forecast using CAPE500 parameterization is due to the production of westerly wind events and not to the different mean state.

The relative contributions of the wind stress and heat flux resulting from the coupled interactions (and depicted in Fig. 9) can also be measured in ocean-only experiments. Results indicate that the wind stress anomaly shown in Fig. 9a (i.e., the wind component of the ''coupled'' interactions) has a small effect: less than 0.5 K on the SST over the equatorial region, less than 5 m in D20, and less than 2 cm in the sea level, and it is not shown. The story is different with the heat flux component of the ''coupled interaction'' (shown in Fig. 9b), which cools the SST anomalies by more that 1.5 K (Fig. 15b). This implies that the anomaly from experiment C_pert (and shown in Fig. 8b) would have been 1.5 K larger towards the end of the integration if there had not been any heat flux response to the SST induced by the imposed wind perturbation. The coupled response in terms of heat flux implies a negative feedback, of strength around 80 W $m^{-2}$ $K^{-1}$, which may be overestimated by the coupled model, as discussed in section 3.

## 6. Conclusions

The present paper explores the impact of the 1997 westerly wind event in May–June 1997 on Niño-3 forecasts with the ECMWF coupled model. It also evaluates the contributions of the different atmospheric fluxes and ocean initial conditions on the SST warming observed during the period May–July 1997.

Coupled forecasts started on 1 May 1997 underestimate the amplitude of the Niño-3 anomalies in July by more than 1 K. The coupled model does not produce strong westerly wind events in the central west Pacific, as observed in May–June 1997. An ensemble of coupled ocean–atmosphere integrations where the observed wind stress anomalies over the tropical Pacific have been added to the wind stress from the atmospheric model produces significantly better forecasts over the Niño-3 region, but still underpredicts the full magnitude of the observed SST anomaly. The coupled model response to this warming is characterized by a negative feedback in terms of heat flux that acts to reduce the SST anomaly.

Experiments in which the threshold for convection of CAPE is increased to 500 J $kg^{-1}$ suggest that improving the representation of transients in the atmospheric component of the GCM significantly improves the forecasts. CAPE500 seems to be beneficial only when westerly wind events significantly impact the Niño-3 SSTs, as was the case in 1997. The choice of a 500 J $kg^{-1}$ CAPE threshold is probably unrealistically high, but these experiments highlight the importance of simulating westerly wind events in a GCM. The present paper also suggests that stochastically perturbing the model physics significantly improves the seasonal forecast of Niño-

3 SSTs, but not as much as with the CAPE500 experiment. This is likely due to the fact that, unlike the integrations with stochastic physics, the CAPE500 integrations seem to display an interannual variability in the occurrence of westerly wind events. The CAPE500 experiments exhibited a more intense intraseasonal variability, extending eastward as far as 160°E.

It would be interesting to determine which aspect of the intraseasonal variability (intensity, location, frequency band) is most influential in ENSO forecasting. Further, it is important to determine the sensitivity of the SSTs to the intraseasonal variability as a function of the ocean initial conditions. Future plans also include investigating the predictability of westerly wind events at intraseasonal and seasonal scales using the CAPE500 parameterization. This will be discussed in a forthcoming paper.

In the coupled experiments, the absence of westerly wind variability only partially explains why the ECMWF seasonal forecasting system failed to predict the strong warming in the Niño-3 region when starting on 1 May 1997. Even when the westerly wind events are included, the Niño-3 forecasts are still well below observations. The response to the wind perturbation is stronger in the ocean-only experiments where no coupled effects are allowed (i.e., variations in heat, momentum, and $P - E$ fluxes are excluded). Ocean-only experiments indicate that the heat flux produced by the coupled model as a response to the SST anomaly causes the equatorial SSTs to cool by more than 1.5 K. The ocean-only experiments also indicate the response of the atmosphere to the warming in the eastern Pacific in terms of winds does not produce any significant effect on the SST. The ocean mean state has some impact on the amplitude of the SST generated by the wind perturbation, but it is not a major contributor to the error in the 1 May forecasts of Niño-3 SST.

Results with ocean-only experiments indicate that the two major contributors to the SST warming during May–July 1997 from forecasts initiated 1 May 1997 were the wind anomaly in the western Pacific and the ocean initial conditions. The anomalous heat flux acted to damp the SST warming, and results suggest that the heat flux estimate might be a source of error in the SST simulation. We are currently investing different ways of reducing this model error.

*Acknowledgments.* The authors would like to thank the two reviewers whose comments proved invaluable in improving the presentation of the material.

## REFERENCES

Barnett, T. P., 1984: Origins of the Southern Oscillation. *Proc. 8th Annual Climate Diagnostics Workshop,* Ontario, Canada, NOAA, 155–158.

——, M. Latif, N. Graham, M. Flugel, S. Pazan, and W. White, 1993: ENSO and ENSO-related predictability. Part I: Prediction of equatorial Pacific sea surface temperature with a hybrid coupled ocean–atmosphere model. *J. Climate,* **6,** 1545–1566.

Barnston, A. G., Y. He, and M. H. Glantz, 1999: Predictive skill of statistical and dynamical climate models in SST forecasts during the 1997–98 El Niño episode and the 1998 La Niña onset. *Bull. Amer. Meteor. Soc.,* **80,** 217–244.

Benestad, R., R. Sutton, and D. L. T. Anderson, 2002: The effect of El Niño on intraseasonal Kelvin waves. *Quart. J. Roy. Meteor. Soc.,* **128,** 1277–1291.

Boulanger, J.-P., and Coauthors, 2001: Role of non-linear oceanic processes in the response to westerly wind events: New implications for the 1997 El Niño onset. *Geophys. Res. Lett.,* **28,** 1603–1606.

Chen, S. S., R. A. Houze Jr., and B. E. Mapes, 1996: Multiscale variability of deep convection in relation to large-scale circulation in TOGA COARE. *J. Atmos. Sci.,* **53,** 1380–1409.

Fedorov, A. V., 2002: The response of the coupled tropical ocean–atmosphere to westerly wind bursts. *Quart. J. Roy. Meteor. Soc.,* **128,** 1–23.

——, S. L. Harper, S. G. Philander, B. Winter, and A. Wittenberg, 2003: How predictable is El Niño? *Bull. Amer. Meteor. Soc.,* **84,** 911–919.

Harrison, D. E., 1984: On the appearance of sustained equatorial westerlies during the 1982 Pacific warm event. *Science,* **225,** 1092–1102.

——, and B. S. Giese, 1991: Episodes of surface westerly wind as observed from islands in the western tropical Pacific. *J. Geophys. Res.,* **96,** 3221–3237.

Keen, R. A., 1982: The role of cross-equatorial cyclone pairs in the Southern Oscillation. *Mon. Wea. Rev.,* **110,** 1405–1416.

Kessler, W. S., 2001: EOF representation of the Madden–Julian oscillation and its connection with ENSO. *J. Climate,* **14,** 3055–3061.

——, and R. Kleeman, 2000: Rectification of the Madden–Julian oscillation into the ENSO cycle. *J. Climate,* **13,** 3560–3575.

Krishnamurti, T. N., D. Bachiochi, T. LaRow, B. Jha, M. Terawi, D. R. Chakraborty, R. Correa-Torres, and D. Oosterhof, 2000: Coupled atmosphere–ocean modeling of the El Niño of 1997–98. *J. Climate,* **13,** 2428–2459.

Kutsuwada, K., and M. McPhaden, 2002: Intraseasonal variations in the upper equatorial Pacific Ocean prior to and during the 1997–98 El Niño. *J. Phys. Oceanogr.,* **32,** 1133–1149.

Landsea, C. W., and J. A. Knaff, 2000: How much skill was there in forecasting the very strong 1997–1998 El Niño? *Bull. Amer. Meteor. Soc.,* **81,** 2107–2120.

Latif, M., and Coauthors, 1998: A review of the predictability and prediction of ENSO. *J. Geophys. Res.,* **103,** 14 375–14 393.

Lin, W.-B., and D. J. Neelin, 2000: Influence of a stochastic moist convective parameterization on tropical climate variability. *Geophys. Res. Lett.,* **27,** 3691–3694.

Lin, X., and R. H. Johnson, 1996: Kinematic and thermodynamic characteristics of the flow over the western Pacific warm pool during TOGA COARE. *J. Atmos. Sci.,* **53,** 695–715.

McPhaden, M. J., 1999: Genesis and evolution of the 1997–98 El Niño. *Science,* **283,** 950–954.

——, 2002: Mixed layer temperature balance on intraseasonal timescales in the equatorial Pacific Ocean. *J. Climate,* **15,** 2632–2647.

Meinen, C. S., and M. J. McPhaden, 2001: Interannual variability in warm water volume transports in the Equatorial Pacific during 1993–99. *J. Phys. Oceanogr.,* **31,** 1324–1345.

Palmer, T. N., 2001: A nonlinear dynamical perspective on model error: A proposal for non-local stochastic-dynamic parametrization in weather and climate prediction models. *Quart. J. Roy. Meteor. Soc.,* **127,** 279–304.

Perigaud, C., and C. Cassou, 2000: Importance of oceanic decadal trends and westerly wind bursts for forecasting El Niño. *Geophys. Res. Lett.,* **27,** 389–392.

Reynolds, R. W., and T. M. Smith, 1994: Improved global sea surface

temperatures analyses using optimum interpolation. *J. Climate*, **7,** 929–948.
Slingo, J. M., 1998: The 1997–98 El Niño. *Weather*, **53,** 274–281.
Smith, N., J. E. Blomley, and G. Meyers, 1991: A univariate statistical interpolation scheme for subsurface thermal analyses in the tropical oceans. *Progress in Oceanography*, Vol. 28, Pergamon, 219–256.
Stockdale, T. N., D. L. T. Anderson, J. O. S. Alves, and M. A. Balmaseda, 1998: Global seasonal rainfall forecasts using a coupled–atmosphere model. *Nature*, **392,** 370–373.
Tiedtke, M., 1989: A comprehensive mass flux scheme for cumulus parameterization in large-scale models. *Mon. Wea. Rev.*, **117,** 1779–1800.
Trenberth, K. E., 1998: Development and forecasts of the 1997–1998 El Niño: CLIVAR scientific issues. *CLIVAR Exchanges*, **3,** 4–14.
van Oldenborgh, G. J., 2000: What caused the onset of the 1997–98 El Niño? *Mon. Wea. Rev.*, **128,** 2601–2607.
Vialard, J., P. Delecluse, and C. Menkes, 2002: A modeling study of salinity variability and its effects in the tropical Pacific Ocean during the 1993–1999 period. *J. Geophys. Res.*, **107,** 8005, doi: 10.1029/2000JC000758.
Vitart, F., J. L. Anderson, J. Sirutis, and R. E. Tuleya, 2001: Sensitivity of tropical storms simulated by a general circulation model to changes in cumulus parametrization. *Quart. J. Roy. Meteor. Soc.*, **127,** 25–51.
Wonnacott, T. H., and R. J. Wonnacott, 1977: *Introductory Statistics*. John Wiley, 650 pp.
Zhang, C., 1996: Atmospheric intraseasonal variability at the surface in the tropical western Pacific Ocean. *J. Atmos. Sci.*, **53,** 739–758.